OXFORD

SOT | Society of Toxicology
www.toxsci.oxfordjournals.org

TOXICOLOGICAL SCIENCES, 142(2), 2014, 497–507

doi: 10.1093/toxsci/kfu202
Advance Access Publication Date: September 25, 2014

In vivo and *In vitro* Toxicity and Anti-Inflammatory Properties of Gold Nanoparticle Bioconjugates to the Vascular System

Mayara Klimuk Uchiyama*, Daiana Kotra Deda*, Stephen Fernandes de Paula Rodrigues†, Carine Cristiane Drewes†, Simone Marques Bolonheis†, Pedro Kunihiko Kiyohara‡, Simone Perche de Toledo‡, Walter Colli§, Koiti Araki*,[1], and Sandra Helena Poliselli Farsky†

*Department of Fundamental Chemistry, Institute of Chemistry, University of Sao Paulo, 05508-000, Sao Paulo, Brazil, †Department of Clinical and Toxicological Analysis, Faculty of Pharmaceutical Sciences, University of Sao Paulo, 05508-000, Sao Paulo, Brazil, ‡Department of General Physics, Institute of Physics, University of Sao Paulo, 05508-090, Sao Paulo, Brazil and §Department of Biochemistry, Institute of Chemistry, University of Sao Paulo, 05508-000, Sao Paulo, Brazil

[1]To whom correspondence should be addressed. Fax: +55 11 3815 5640. E-mail: koiaraki@iq.usp.br

ABSTRACT

Gold nanoparticle (AuNP) bioconjugates have been used as therapeutic and diagnostic tools; however, *in vivo* biocompatibility and cytotoxicity continue to be two fundamental issues. The effect of AuNPs (20 nm) conjugated with antibody [immunoglobulin G (IgG)], albumin, protein A, PEG4000, and citrate (*cit*) were evaluated *in vitro* using primary human cells of the vascular system. AuNP bioconjugates did not cause lysis of human erythrocytes, apoptosis or necrosis of human leukocytes, and endothelial cells *in vitro*, although AuNPs had been internalized and detected in the cytoplasm. Moreover, the influence of AuNPs on rheological parameters, blood and vessel wall characteristics was investigated *in vivo* by intravital microscopy assay using male Wistar rats mesentery microcirculation as model. Intravenous injection of AuNP-IgG or *cit*-AuNP did not cause hemorrhage, hemolysis or thrombus formation, instead suppressed the leukocyte adhesion to postcapillary vessel walls, an early stage of an inflammatory process. Furthermore, AuNP-IgG abrogated the expression of platelet-endothelial cell adhesion molecule-1, chemotaxis, and oxidative burst activation on neutrophils after leukotriene B4 stimulation, a membrane receptor-dependent stimulus, thus confirming their anti-inflammatory effects *in vitro*. The expression of oxidative burst activation was also suppressed after stimulating AuNP-IgG-treated neutrophils with lipid-soluble phorbol myristate acetate (PMA), confirming the direct intracellular action of AuNP-IgG on the inflammatory process *in vitro*. Our *in vitro* and *in vivo* experimental approaches highlighted the great potentiality of AuNP bioconjugates for therapeutic and diagnostic applications by parenteral routes.

Key words: cytoviva; leukocyte-endothelial interactions; intravital microscopy; neutrophils; human leukocytes; erythrocytes

Gold nanoparticles (AuNPs) conjugated with biomolecules have been explored since 1971, when Faulk and Taylor (1971) used for the first time AuNP-immunoglobulin G (AuNP-IgG) bioconjugates as direct immunocytochemical probes to identify the antigens present in *Salmonella* surface. Nowadays, AuNPs have been investigated for application in diagnosis, vector transfection, drug and gene delivery, treatment by hyperthermia, and as probes for imaging (Park *et al.*, 2009), exploring their unique optical and binding properties (Liz-Marzan, 2004). Also, interesting applications have been envisaged for the development of new diagnostic methods, by associating AuNPs with surface-enhanced Raman scattering (Grasseschi *et al.*, 2010) and surface Plasmon resonance spectroscopy (Choi *et al.*, 2008).

Nevertheless, controlling the structure and understanding the interaction of nanobioconjugates with cells are formidable tasks. In fact, the unique physical, chemical, and mobility properties of nanoparticles (NPs) at cellular and molecular levels control their biodistribution and pharmacokinetics (Daniel and Astruc, 2004). These are essential for the right balance of pharmacological and toxicological activities, responsible for the therapeutic efficacy and suitability for *in vivo* application. In this context, the surface functionalizing molecules play key roles, as polyethylene glycol (PEG) improves the half-life of nanobiomaterials in blood (de Assis *et al.*, 2008), IgG confers targeting properties (Bleher *et al.*, 2008), bovine serum albumin (BSA) helps avoid non-specific bonding, and protein A attaches specifically to the Fc region of antibodies (Forsgren and Sjoquist, 1966).

Although NPs have been successfully employed in biological applications, their toxic effects have not being completely elucidated yet (Stefan *et al.*, 2013). Kinetics of uptake, distribution, and excretion of NPs, as well as their mechanisms of action, may not be correlated with the well-defined parameters of bulk materials (Pattan and Kaul, 2012). Thus, the Organization for Economic Cooperation and Development (OECD) reinforced that health and safety regulations remain undefined for NPs (Lauterwasser, 2005). In fact, several current studies have reported the toxicity and injuries caused by AuNPs to biological systems, fueling the controversy and discussions about the safety of those nanomaterials (Paino *et al.*, 2012; Siddiqi *et al.*, 2012).

Because of the size similarity with cell components and proteins, AuNPs may pass through vessel walls and eventually through the blood-brain barrier (Sonavane *et al.*, 2008). Thus, the toxicity seems to depend on size, shape, chemical composition, charge, and agglomeration state of NPs (Kong *et al.*, 2011). However, the stability, dispersability, and interaction properties are mainly controlled by the nature of surface functionalizing molecular layer (Stefan *et al.*, 2013). The cytotoxicity dependence on the shape was explored by Tarantola *et al.* (2009) who showed that spherical NPs are more toxic and easily internalized than rod-shaped ones, by monitoring epithelial cells incubated with cetyltrimethylammonium bromide (CTAB)-coated gold spheres and rods. Paino *et al.* (2012) pointed out that citrate and polyamideamine-coated AuNPs exhibit concentration-dependent cytotoxicity and genotoxicity toward HepG2 carcinoma cells. Goodman *et al.* (2004) showed that cationic AuNPs are moderately cytotoxic in contrast with their anionic counterparts, as expected from the higher electrostatic interaction with biomolecules. On the other hand, 14–100-nm citric acid-coated AuNPs were uptaken by HeLa cells but did not cause cellular death (Chithrani *et al.*, 2006). Similar results were reported by Connor *et al.* (2005) for 4-nm cysteine- and citrate-capped, 12-nm glucose-reduced, and 18-nm citrate-, biotin-, and CTAB-hybridized gold spheres, which were non-toxic to human leukemia cells. Also, polyvinylpyrrolidone-coated 5-nm large AuNPs were biocompatible with rat liver cells (Dragoni *et al.*, 2012). Moreover, systemic administration of AuNPs was shown to cause both pro and anti-inflammatory activities (Chen *et al.*, 2013; Khan *et al.*, 2013). Moreover, effects of AuNPs on inflammation are controversial and may be dependent on physicochemical properties. Intraperitoneal injection of AuNPs (21 nm) into C57BL/6 mice reduced the levels of mRNA interleukin-6 (IL-6) and tumor necrosis factor (TNF-α) in the abdominal fat pad (Chen *et al.*, 2013). On the other hand, injection of AuNPs (10 or 50 nm) into peritoneal cavity of Wistar-Kyoto rats increased the gene expression of cytokines in the liver (Khan *et al.*, 2013).

The first contact of IV-administered chemicals, within a host organism, is always with blood components and the inner layers of vascular walls. Considering the functional and metabolic relevant action of both blood and vessel cells, toxic effects frequently impair the homeostasis and may lead to several diseases, including thrombosis, coagulation, inflammation, immunosuppression, and hypertension (Berger, 2013). Although the administration of AuNPs by IV routes has been proposed, to the best of our knowledge, there is no report on their effect on the vascular system, particularly on the interaction with erythrocytes, leukocytes, and vessel wall cells in the microcirculation. To fill this gap, the *in vitro* and *in vivo* effects of AuNP bioconjugates on blood cells and microvascular system were investigated. AuNPs did not cause vessel and blood cells death, nevertheless inhibited the leukocyte-endothelial microvascular interactions and neutrophil functions.

MATERIALS AND METHODS

Roswell Park Memorial Institute (RPMI) 1640 medium Trypsin-ethylenediamine tetraacetic acid (EDTA) solution, and fetal bovine serum (FBS) were purchased from Vitrocell (Campinas, SP, Brazil). Ficoll-Hypaque, lipopolysaccharide from *Escherichia coli* (LPS, serotype 026:B6), leukotriene B4 (LTB4), phorbol myristate acetate (PMA), 2′,7′-dichlorofluorescein diacetate (DCFH-DA), sulfanilamide, naphthyl ethylenediamine dihydrochloride, propidium iodide (PI), sodium citrate, dextran, BSA, PEG (wt 4000, PEG4000), Triton X-100, paraformaldehyde, osmium tetroxide (OsO_4), uranyl acetate, oyster glycogen, and trypan blue were acquired from Sigma (St. Louis, MO). Protein A was acquired from Molecular Probes, Life Technology. Heparin was purchased from Eurofarma (São Paulo, Brazil); and Annexin-V conjugated with fluorescein isothiocyanate (FITC) was purchased from BD Pharmingen (San Diego, CA). Human umbilical vein endothelial cells (HUVECs) were obtained from the American Type Culture Collection (Manassas, VA). Anti-β_2-integrin and anti-PECAM-1 were obtained from BD (Becton&Dickinson). Dopalen® and Anasedan® were purchased from Vetbrands (Brazil).

All experimental procedures involving animals were reviewed and approved by the Internal Animal Care and Use Committee of Institute of Chemistry, University of Sao Paulo, Sao Paulo, Brazil, and performed according to the criteria outlined by the Ethical Principles in Animal Research adopted by Conselho Nacional de Controle de Experimentação Animal (CONCEA) (Protocol number: 15/2012). For assays employing human blood cells, written consent was obtained from all healthy volunteers before blood collection.

Synthesis and Characterization of AuNP Bioconjugates. Citrate-protected AuNPs (*cit*-AuNP) were prepared by adding 3 ml of 1% sodium citrate solution in $HAuCl_4$ boiling solution (16 mg/100 ml of 18.2 MΩ.cm^{-1} Milli-Q DI-water) under vigorous stirring (Turkevich *et al.*, 1951). The AuNP bioconjugates were prepared by reacting the *cit*-AuNP suspension with suitable amounts of mouse monoclonal anti-H3.3 antibodies from hybridoma culture, BSA, protein A, and PEG4000 dispersed in DI-water (18.2 MΩ.cm^{-1}). They must cover the AuNPs surface to avoid aggregation. Thus, the suitable amounts depend on the size and charge of those biomolecules.

UV-Vis spectra were registered in a diode-array HP8453A spectrophotometer. The NPs size distribution and zeta potential were measured by dynamic light scattering (DLS) using a *Malvern* ZEN3600 Zetasizer Nano ZS equipped with a 633-nm laser. Transmission Electron Microscopy (TEM) images were obtained in a Philips CM200 electron microscope, operating at 160 kV. The samples were prepared by depositing the nanomaterials on copper grids covered with a carbon film.

Toxicity on Vascular System Human Cells. The cytotoxic effects of AuNP bioconjugates on the vascular system were evaluated using circulating human leukocytes and erythrocytes and HUVEC. Human mono (PBMC) and polymorphonuclear (PMN) cells were isolated as described by Boyum (1968).

HUVEC grown in culture flasks and maintained in RPMI 1640 were supplemented with 10% FBS. Cells were kept at 37°C, at minimum relative humidity of 95%, and atmosphere of 5% of CO_2 in air.

In order to investigate the cytotoxicity, 1×10^6 PMN or PBMC/well or 1×10^5 HUVEC/well were seeded in 24-well plates with 400 μL of RPMI culture media plus 10% FBS (R10), and incubated with 100 μL of AuNP bioconjugates (about 1×10^{11} particles) or the respective functionalizing molecules (solution in DI-water) during 18 h, at 37°C. Then, cells were incubated for 20 min with annexin-V FITC (1:100 v/v) and PI (10 μL, 50 μg/ml); and analyzed in a FACS Canto II flow cytometer (Becton&Dickinson). In order to guarantee the efficacy of assays, ethanol and DMSO were used as positive control for apoptosis and necrosis, respectively. Data from 10,000 events were analyzed and the results expressed as percentage of necrotic, apoptotic, late apoptotic (dual labeling), and viable cells.

Red blood cells (RBCs) were incubated with AuNP bioconjugates and the hemolytic activity was evaluated according to the method described by Sharma and Sharma (2001). Briefly, human blood was collected in 0.13 M sodium citrate solution in PBS, centrifuged (1300 × g, 15 min), and RBCs were collected and washed with PBS. The pellet was resuspended in PBS, in a final concentration of 10% v/v of RBC; 500-μL aliquots were incubated with 100 μL of AuNP bioconjugates (about 1×10^{11} NPs) for 1 h, at 37°C, under orbital stirring. Optical density (OD) of the supernatant obtained after centrifugation was monitored at 540 nm (Spectramax Plus 384, Molecular Devices Inc., Sunnyvale). The positive control (100% hemolysis) was prepared incubating 500 μl of RBC suspension with 100 μl of 0.2% Triton X-100 solution in DI-water. The background absorbance of AuNP bioconjugate was evaluated in their respective suspensions (500 μl PBS and 100 μl of each AuNP bioconjugate) and subtracted from the absorbance of the sample at 540 nm. Besides, a negative control to correct the baseline of all samples was also prepared incubating 500 μL of RBC suspension with 100 μL of DI-water, the dispersion medium of NPs. The percentage of AuNP bioconjugate-induced hemolysis was calculated as follows: %hemolysis = 100 × (Abs sample/Abs total hemolysis by triton X-100), where Abs = absorbance, and also making the necessary corrections from each control described above. The baseline RBC lysis induced by the biomolecules in analogous RBC-PBS suspensions (500 μl RBC in 100 μl PBS) was insignificant.

In vitro *Cellular Uptake*. Microscopy studies were carried out to confirm the possible internalization of AuNPs by cells using human circulating leukocytes, HUVEC, and rat neutrophils incubated with 400 μl of RPMI culture media plus 10% FBS, containing 100 μl of *cit*-AuNP or AuNP-IgG (about 1×10^{11} NPs), during 18 h.

PBMC and PMN cells were fixed with 2% paraformaldehyde in PBS for 2 h at 4°C, post-fixed with 1% OsO_4 in 0.1 M PBS for 1 h, washed with PBS and centrifuged (1300 × g, 15 min). The cells pellet was stained with 2% uranyl acetate for 30 min at 60° C, rinsed three times with deionized water, dehydrated with solutions with progressively higher concentrations of ethanol, then in 100% propylene oxide, and embedded in epoxy resin. Thin sections, cut using a Reichert Ultracut E Ultramicrotome, were placed on 200 mesh copper grids and stained with lead citrate. Images of the PBMC and PMN cells were obtained using a JEOL 1010 transmission electron microscope operating at 100 kV.

Rat neutrophils (obtained 4 h after i.p. injection of 1% oyster glycogen solution) and HUVEC were imaged using a combination of dark-field reflectance and hyperspectral imaging. Dark-field reflectance microscopy and hyperspectral images were acquired in a CytoViva Ultra Resolution Imaging System mounted on an Olympus BX51 microscope. The same 0.5 NA objective and a 75W Xe light source were used throughout. The hyperspectral system was calibrated using a standard wavelength calibration lamp (low pressure Hg, Lightform, Inc.). The images were normalized using the Xe lamp spectrum on a pixel-by-pixel basis. Red-green-blue images were taken with a Q-imaging Retiga EXi CCD camera, with color LCD attachment under identical conditions, and white balanced with the Spectral on Image Processing Software (Labsphere, North Sutton, New Hampshire). A minimum of 50 cells was analyzed per time point.

In vivo *Alterations on Microvascular System and Anti-Inflammatory Effects*. Male Wistar rats (300–400 g) were divided into five groups, according to the IV treatments: (1) Saline (0.9% sodium chloride); (2) DI-water; (3) IgG dissolved in DI-water; (4) *cit*-AuNP; and (5) AuNP-IgG. After subcutaneous anesthesia with ketamine (100 mg/kg)/xylazine (10 mg/kg) solution, left femoral vein was cannulated and a single 1 ml dose of each treatment injected IV, at an infusion rate of 500 μl/min. AuNPs stock suspension (about 1×10^{12} NPs/ml, 8×10^{-5} g Au/ml) was dispersed in DI-water, which also was used as control in our experiments along with saline solution. The AuNP-IgG bioconjugate (AuNPs coated with monoclonal antibody against *Trypanosoma cruzi* trypomastigotes) (Giordano *et al.*, 1999) was chosen to evaluate the influence of a large biomolecule on the toxicological properties of AuNPs in the vascular system.

Medial laparotomy was done on cannulated rats and the mesentery was exteriorized for *in situ* microscopic examination. Animal surgery and maintenance of mesentery microcirculation were carried out following the protocols described by Macedo *et al.* (2006) and de Lima *et al.* (2012).

Influence of AuNPs on leukocyte migration from the interior of blood vessels to the tissue parenchyma was quantified. The integrated number of adherent (per 100 μm of venule) and migrating leukocytes (in a 5000 μm^2 standard area of connective

tissue adjacent to a post-capillary venule) was determined as a function of time (before, just after, and 0.5, 1, 1.5 and 2 h after injection). Three different vessels were evaluated and the results averaged for each animal to avoid sampling-associated variability.

Another set of assays was carried out to investigate the anti-inflammatory effect of AuNP-IgG evoked by topical application of LTB4 (10^{-9} M). AuNP-IgG was IV-administered 30 min before LTB4 stimulation. The number of adherent leukocytes was evaluated, at different intervals of time, as described above.

Effects of AuNPs on Neutrophil Functions: Anti-Inflammatory Activities. Neutrophils were obtained from anesthetized rats 4 h after i.p. injection of 10 ml of 1% sterile oyster glycogen solution. The number of viable cells (98%) was counted in a hemocytometer chamber using an optical microscope (Nikkon, Japan). Neutrophils (1×10^5 cells/well) were treated with RPMI plus 10% FBS (R10, control), citrate supernatant (cit), IgG, *cit*-AuNP and AuNP-IgG (about 1×10^{11} NPs/100 μL) and employed for chemotaxis, burst oxidative and adhesion molecules expression assays.

The migratory assay was performed using a multi-well chemotaxis chamber, and filters with 8 μm pore size (Chemo TX System, Neuro Probe), as previously described by de Lima *et al.* (2012). In summary, the bottom wells of the Boyden chamber were filled with LTB4 or HBSS and neutrophils were placed in the top wells, and incubated during 2 h (37°C; 5% CO_2). The filters were removed and the number of migrated neutrophils was determined by optical microscopy (Nikkon) in a hemocytometer chamber.

AuNPs-treated neutrophils were incubated with LTB4 (1×10^{-8} M) or PMA (1×10^{-8} M) or R10 (2 h, 37°C), washed with HBSS and the intracellular reactive oxygen species (ROS) was measured with DCFH-DA, a non-fluorescent probe that penetrates into the intracellular matrix, where it is oxidized to the highly fluorescent dichlorofluorescein species. The cells were resuspended in DCFH-DA (10 μM; diluted in PBS), transferred to a 96-well plate and maintained at 37°C for 30 min. After this period, the fluorescence was analyzed using a plate reader with $\lambda_{exc.}$= 488 nm and $\lambda_{emi.}$= 530 nm (SynergyH1, Hybrid Reader, BioTek). Results are presented in arbitrary fluorescence units.

Neutrophils treated with AuNPs were simultaneously stimulated with LTB4 (1×10^{-8} M, 1 h, 37°C) and R10. Then, cells were washed and incubated with monoclonal antibody anti-PECAM-1 conjugated with PE or anti-β_2-integrin conjugated with FITC, at 4°C. Twenty minutes later, cells were analyzed on a FACS Canto II flow cytometer. Data from 10,000 events were obtained. Results were expressed as mean of fluorescence intensity.

Statistical analysis. All data were expressed as average ± s.e.m. Statistical differences between the groups were determined by one-way analysis of variance (ANOVA) applying the Tukey's post hoc test implemented in Prism 5 software (GraphPad Software, Inc.). Statistical significance was set at $P < .05$.

RESULTS

Characterization of AuNP Bioconjugates

The starting *cit*-AuNP has an average diameter of approximately 20 nm according to DLS measurements, but that average hydrodynamic radius increased when the relatively small citrate molecules were replaced by larger biomolecules (Table 1). The stock solution concentration was estimated as 1×10^{12} particles/ml (8×10^{-5} g Au/ml) from the amount of tetrachloroauric acid used in the synthesis, and the average number of gold atoms in 20 nm diameter AuNPs, as determined by TEM (Supplementary Figs. S1A and B), considering the density of 59 gold atoms per nm^3 (details in Supplementary Data).

TABLE 1. Average Size and Zeta Potential of *cit*-AuNP and AuNP Bioconjugates

Particle	Size*/nm	Zeta potential*/mV
cit-AuNP	20.60	−10.4
AuNP-IgG	46.70	−26.4
AuNP-BSA	25.85	−19.7
AuNP-Protein A	27.03	−19.7
AuNP-PEG4000	22.31	−6.47

*Size and zeta potential were expressed as averages with maximum deviation of 20%.

AuNP bioconjugates were prepared controlling the concentration of hybridizing molecules in solution in order to get stable colloidal suspensions, as confirmed by the single plasmon band around the wavelength of 520 nm (Supplementary Fig. S1C), and the small broadening induced by the functionalization of the AuNP surface. The colloidal stability can be explained by the relatively high negative zeta potentials of the bioconjugates (Table 1) as compared with *cit*-AuNP, reflecting a lower tendency to agglomerate, as confirmed by TEM (Supplementary Figs. S1A and B). The exception was the AuNP-PEG4000 conjugate, which exhibited approximately 60% less negative zeta potential.

Toxicity on Human Cells of Vascular System

The ability of *cit*-AuNP and their bioconjugates to disrupt the cell membrane of circulating leukocytes inducing toxicity was initially verified by Trypan Blue exclusion test (Supplementary Fig. S2). However, AuNPs did not induce any alteration on the membrane, as >95% of PBMC and about 80% of PMN cells were found to be viable. Also, no significant differences were found in R10- and AuNPs-treated cells. However, AuNPs may cause cell death without disrupting the membrane. In order to investigate this possibility, further cytotoxicity assays were carried out measuring cell apoptosis and necrosis. The percentage of necrotic, apoptotic and late apoptotic PBMC and PMN cells (Table 2) were found to be very low and indistinguishable from the respective controls. Control experiments for the influence of surface functionalizing molecules/biomolecules (Supplementary Fig. S3), serum and RMPI (Supplementary Fig. S4) on cell viability were also carried out, but no significant effect was found. Furthermore, AuNPs did not alter intracellular pathways involved in the PBMC or PMN cell secretion, such that the levels of secreted TNF were equivalent in the controls and cells treated with all AuNP bioconjugates (Supplementary Fig. S5). A slight increase in nitric oxide levels was observed after incubation of PBMC with *cit*-AuNP, AuNP-BSA or AuNP-PEG4000, and after incubating PMN with *cit*-AuNP. However, the differences are lower than 5 μM, and probably are not related to any toxic effect.

Endothelial cells coating the vessel walls are in direct contact with circulating species, such as IV-administered chemicals. However, AuNP conjugates did not cause any toxic effect in HUVEC, as confirmed by absence of apoptosis or necrosis (Table 2).

It is noteworthy that toxic effects were not observed even when NPs interacted and were internalized by PBMC and PMN

TABLE 2. Effects of AuNP Bioconjugates on Cytotoxicity

		Viability (%)	Apoptosis (%)	Late apoptosis (%)	Necrosis (%)
PBMC*	R10	91.48 ± 1.85	0.78 ± 0.42	1.23 ± 0.68	6.52 ± 2.52
	cit-AuNP	88.18 ± 6.32	0.47 ± 0.34	0.98 ± 0.76	10.37 ± 6.80
	AuNP-IgG	90.45 ± 1.88	0.97 ± 0.54	1.66 ± 0.92	6.91 ± 2.75
	AuNP-BSA	90.53 ± 3.55	0.72 ± 0.60	1.08 ± 0.88	7.67 ± 3.98
	AuNP-Protein A	93.27 ± 0.55	1.15 ± 0.55	1.64 ± 0.94	3.97 ± 0.99
	AuNP-PEG4000	92.43 ± 1.02	0.49 ± 0.29	0.84 ± 0.47	6.22 ± 1.29
PMN**	R10	87.73 ± 3.41	7.06 ± 5.20	0.58 ± 0.34	4.66 ± 1.61
	cit-AuNP	85.23 ± 6.04	8.35 ± 6.67	2.44 ± 2.26	4.00 ± 0.69
	AuNP-IgG	88.38 ± 3.76	7.08 ± 5.66	0.73 ± 0.50	3.81 ± 1.00
	AuNP-BSA	88.65 ± 3.25	4.02 ± 2.55	1.72 ± 1.47	5.62 ± 1.32
	AuNP-Protein A	86.05 ± 2.33	5.79 ± 3.32	1.61 ± 0.88	6.55 ± 0.66
	AuNP-PEG4000	90.70 ± 1.09	4.03 ± 2.17	0.71 ± 0.29	4.56 ± 0.77
HUVEC***	R10	86.84 ± 3.59	0.45 ± 0.40	2.39 ± 2.01	11.46 ± 3.50
	cit-AuNP	85.77 ± 5.54	0.48 ± 0.43	3.87 ± 3.52	9.16 ± 2.72
	AuNP-IgG	88.26 ± 3.43	0.33 ± 0.27	1.69 ± 1.40	9.86 ± 2.38
	AuNP-BSA	89.39 ± 2.79	0.11 ± 0.10	0.38 ± 0.09	9.22 ± 2.01
	AuNP-Protein A	89.70 ± 2.57	0.05 ± 0.03	0.20 ± 0.05	5.19 ± 0.43
	AuNP-PEG4000	92.00 ± 1.10	0.03 ± 0.00	0.28 ± 0.23	6.39 ± 0.98

*PBMCs were isolated from four healthy male volunteers.
**PMN were isolated from five healthy male volunteers.
***DMSO 10% was employed as a positive death control. Cells from three independent HUVEC cultures were employed in the assay.
Percentage of necrotic, apoptotic, late apoptotic, and viable PBMC, HUVEC and PMN cells after 18 h of incubation with R10 (control) or AuNP bioconjugates, evaluated by flow cytometry.

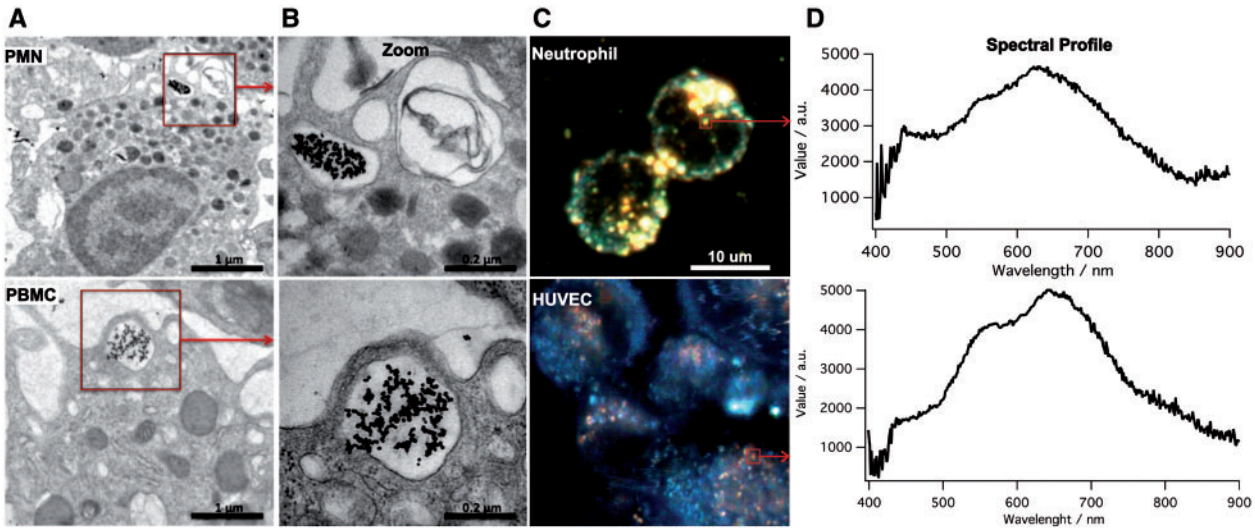

FIG. 1. Representative images of human PBMC and PMN cells, rat neutrophils and human umbilical vein endothelial cells (HUVEC) incubated with *cit*-AuNP for 18 h. A, TEM images of PMN cells (above) and PBMC (below). B, Corresponding Images showing magnified views of the areas indicated in 'A'. C. CytoViva images of rat neutrophils and HUVEC cells. D. Spectrum of the area containing AuNPs indicated in 'C' for neutrophils cells and HUVEC, respectively.

cells. As shown in Figs. 1A and B, both human circulating leukocytes contain vesicles with NPs inside, probably endosomes, forming agglomerates of variable shapes and sizes after incubation with *cit*-AuNP for 18 h. Similarly, aggregated AuNPs were found in the cytoplasm of rat neutrophils and HUVEC (Fig. 1C), as confirmed by the characteristic AuNPs plasmon coupling bands with maxima at 550 and 700 nm shown in Fig. 1D.

The hemolytic properties of AuNP bioconjugates and respective functionalizing molecules/biomolecules were found to be insignificant after incubating them with human RBCs, as shown in Fig. 2. Note that in all cases, the percentage of hemolysis remained below 1% in comparison with Triton X-100 used as a positive control.

In vivo *Alterations on the Microvascular System*

Considering that AuNP bioconjugates did not exhibit toxic effects in all *in vitro* assays described above, a quite sensitive *in vivo* assay was chosen as a final toxicity test. Intravital microscopy studies were carried out to evaluate the effect of AuNPs on the vessel hemodynamics of rat mesentery microcirculation. The assays were carried out only with *cit*-AuNP, AuNP-IgG and their specific controls in order to minimize the number of sacrificed animals.

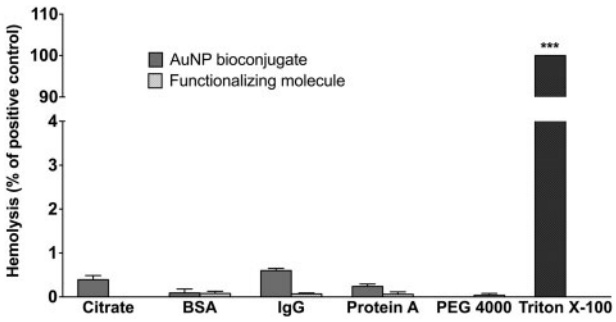

FIG. 2. Hemolytic activity of gold nanoparticles (AuNP) bioconjugates on human cells, collected from three healthy male volunteers, incubated with AuNP bioconjugates and Triton X-100 (positive control) for 1 h. Hemolytic activity was measured spectrophotometrically at 540 nm. ***$P < .001$ versus all other groups.

Injection of AuNPs caused no change in the blood flow velocity (Supplementary Fig. S6A), did not increase the number of micro-hemorrhages (Supplementary Fig. S6B), and induced no thrombus, as compared with saline used as control, within 2 h of observation.

On the other hand, IV injection of DI-water enhanced the number of adhered and migrated leukocytes 2 h later, as shown in Figs. 3A and B, respectively. Interestingly, injection of *cit*-AuNP and AuNP-IgG did not cause the same effect, as the corresponding vehicle. In fact, the number of adherent and migrating cells in AuNP-treated animals was lower than those determined in saline-treated animals (Figs. 3A and B). This implies that AuNPs, in special AuNP-IgG, reduced the leukocyte-endothelial interactions, suggesting a possible anti-inflammatory effect.

Therefore, another set of assays was carried out to evaluate the relevance of AuNP-IgG on endothelial-leukocyte interactions evoked by an inflammatory stimulus. The topical application of LTB4 to mesentery network induced a local stimulation characterized by leukocyte adhesion to the vessel walls, but the effect was prevented by previous injection of AuNP-IgG, as shown in Figs. 4A and B.

Effects of AuNPs on Neutrophil Functions

To clarify the mechanism of AuNP-IgG anti-inflammatory activity, the expression of adhesion molecules, chemotaxis and oxidative burst were quantified in treated neutrophils.

LTB4 treatment enhanced the expression of PECAM-1 (and β_2-integrin) on neutrophil membranes after 1 h incubation in the control experiment, but that overexpression was abrogated by treatment with AuNP-IgG (Figs. 5A and B). In addition, AuNP-IgG treatment inhibited the LTB-4-induced neutrophil chemotaxis and ROS generation (Figs. 5C and D). In fact, the ROS generation induced by PMA was also inhibited by AuNP-IgG (Fig. 5D).

DISCUSSION

To our knowledge, we here showed for the first time the *in vivo* behavior of AuNP bioconjugates on the vascular system after IV administration, demonstrating that their interaction with blood and vessel wall cells does not cause cell death but rather evokes anti-inflammatory effects, by reducing leukocyte-endothelial interactions and neutrophil locomotion into tissue. The data presented herein contribute to widen the knowledge on AuNP bioconjugates aiming the development of bionanomaterials for clinical application.

UV-vis spectroscopy, DLS and zeta potential measurements were initially employed to characterize AuNPs suspensions, showing that the colloidal stability of nanobioconjugates is mainly defined by the nature of the biomolecule and surface coverage. Nevertheless, the interaction of AuNPs with biomolecules may occur by two main mechanisms: (1) substitution of citrate molecules and direct binding to the surface or (2) electrostatic interaction of positively charged residues with the negatively charged *cit*-AuNP. Both are important factors but stronger bonds are expected in the former case leading to more stable bioconjugates.

Both AuNPs and biomolecules are potential bridging species. Thus, *cit*-AuNP was added into the biomolecule solution under stirring to assure as fast as possible binding and formation of dispersed hybrid AuNPs. The success of this strategy was confirmed by UV-vis spectroscopy and DLS measurements. As expected, the results were consistent with AuNP bioconjugates whose sizes are the sum of the NP core diameter and two times the protein or polymer shell thickness. Another evidence is their low tendency to agglomerate as compared with *cit*-AuNP, as shown in the TEM images.

Generally, the simple binding of molecules onto AuNP surface induces only a small broadening of the plasmon band at 520 nm. This contrast with the spectral changes taking place upon aggregation (Araki *et al.*, 2006) where a new broad band appears in the 600–900 nm range, depending on how strongly the localized plasmons are coupled.

Aggregation can be induced by increasing the ionic strength and by changing the pH, lowering the electrostatic repulsion between the NPs. However, the concentration of biomolecules in solution was controlled in such a way to assure completely dispersed and stable AuNP bioconjugate suspensions, even in PBS. In fact, the centrifuged pellet could be resuspended in that same solution without significant aggregation. This high colloidal stability can be explained by the twice as large negative zeta potential of the AuNP bioconjugates, as compared with *cit*-AuNP. The exception was AuNP-PEG4000, with approximately 60% less negative zeta potential, indicating that some citrate molecules remained bond to the surface stabilizing them by steric and electrostatic effects.

After IV injection, AuNPs interact with blood and vessel wall cells. Both circulating leukocytes and erythrocytes, as well as the endothelial cells coating the vessel walls, present high functional and metabolic activities, which are pivotal for homeostasis and host defense. Therefore, changes on the expression/activity of cell membrane or intracellular receptors, and up- or downregulation of intracellular metabolic pathways, may lead to several immune, hematological and vascular diseases (Bkaily *et al.*, 2014). Our data clearly show that any of the AuNP bioconjugates causes no apoptosis or necrosis of human leukocytes and endothelial cells, neither alters the ability of PBMC and PMN cells to secrete TNF-α. The lack of toxicity does not mean that AuNP bioconjugates has no or deficient interaction with cells, because they were found in the cytoplasm of HUVEC, PBMC, and PMN cells. Nevertheless, no hemolysis was observed. Summarizing, our data suggest that AuNP bioconjugates may be compatible with blood cells, however, functional and morphological parameters must be further analyzed to confirm the absence of cytotoxicity. In this context, He *et al.* (2014) showed that PEGylated AuNPs also cause no hemolysis but accelerated erythrocyte senescence process.

Although *in vitro* assays have been fully employed to evaluate the toxicity of chemicals, *in vivo* experiments highly contributed to shed light on the toxic effects because they are based

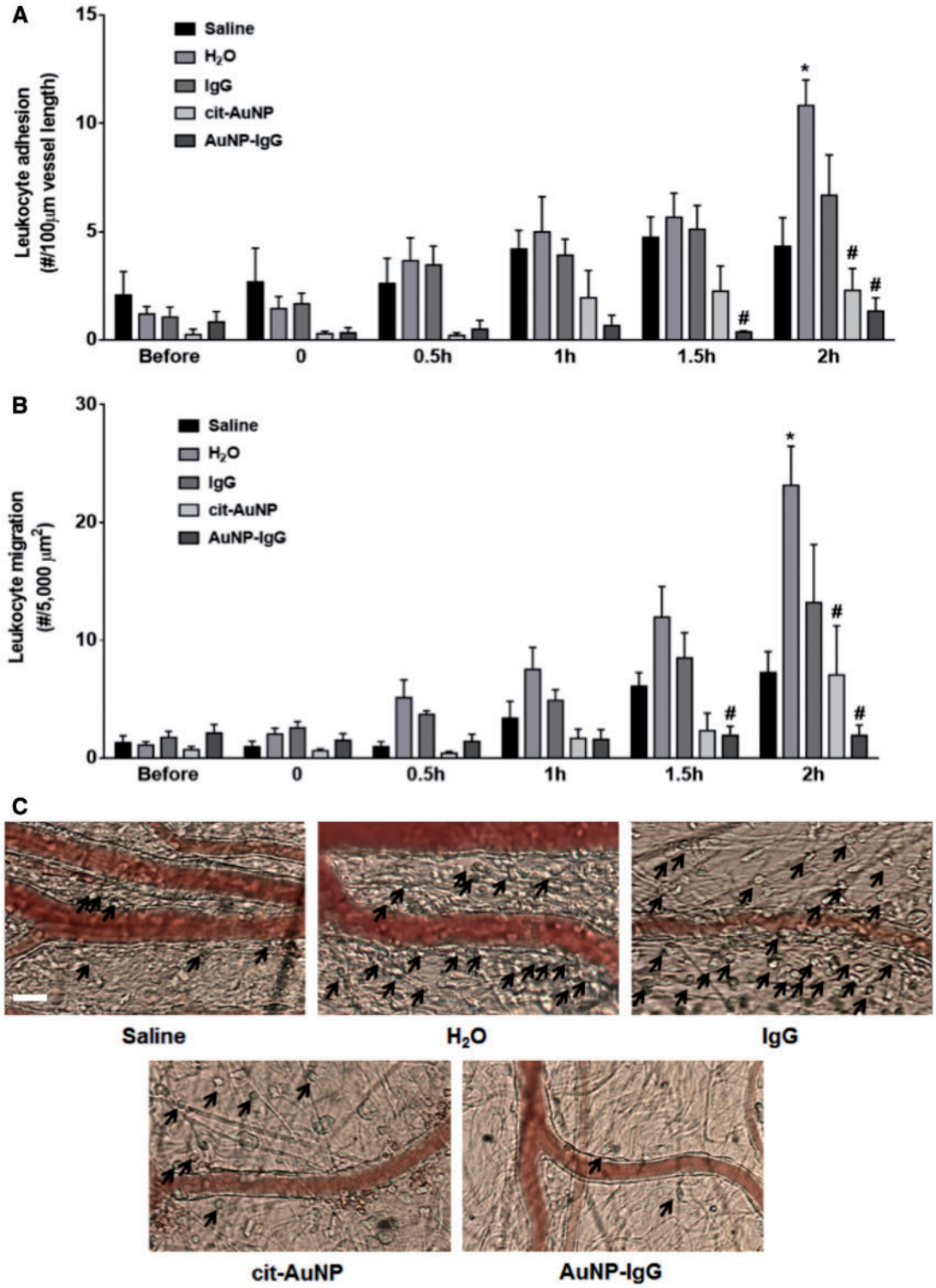

FIG. 3. Effects of gold nanoparticles (AuNP) bioconjugates on leukocyte-endothelial interactions evaluated in male Wistar rat mesentery microcirculation by intravital microscopy. Number of adhered (A) and migrated leukocytes (B) along the mesentery vessel walls before and 0.5–2 h after treatments. Representative images of mesenteric vascular beds after treatments (C). Black arrows indicated adhered and migrated leukocytes. White bar = 20 μm. Values express the average data obtained from four to seven animals in each group. *$P < .05$ versus respective saline treatment; #$P < .05$ versus respective treatment with water.

on more complex models approaching the actual situation. This allows considering the interaction of AuNPs with the whole blood constituents and its rheological properties, as well as the complex effects on the vessel walls endothelial cells that could change their toxic effects. Therefore, we translated our studies to a rat model in order to investigate the AuNPs dynamics on *in vivo* microcirculation by intravital microscopy, after intravenous injection. Our results confirmed the absence of

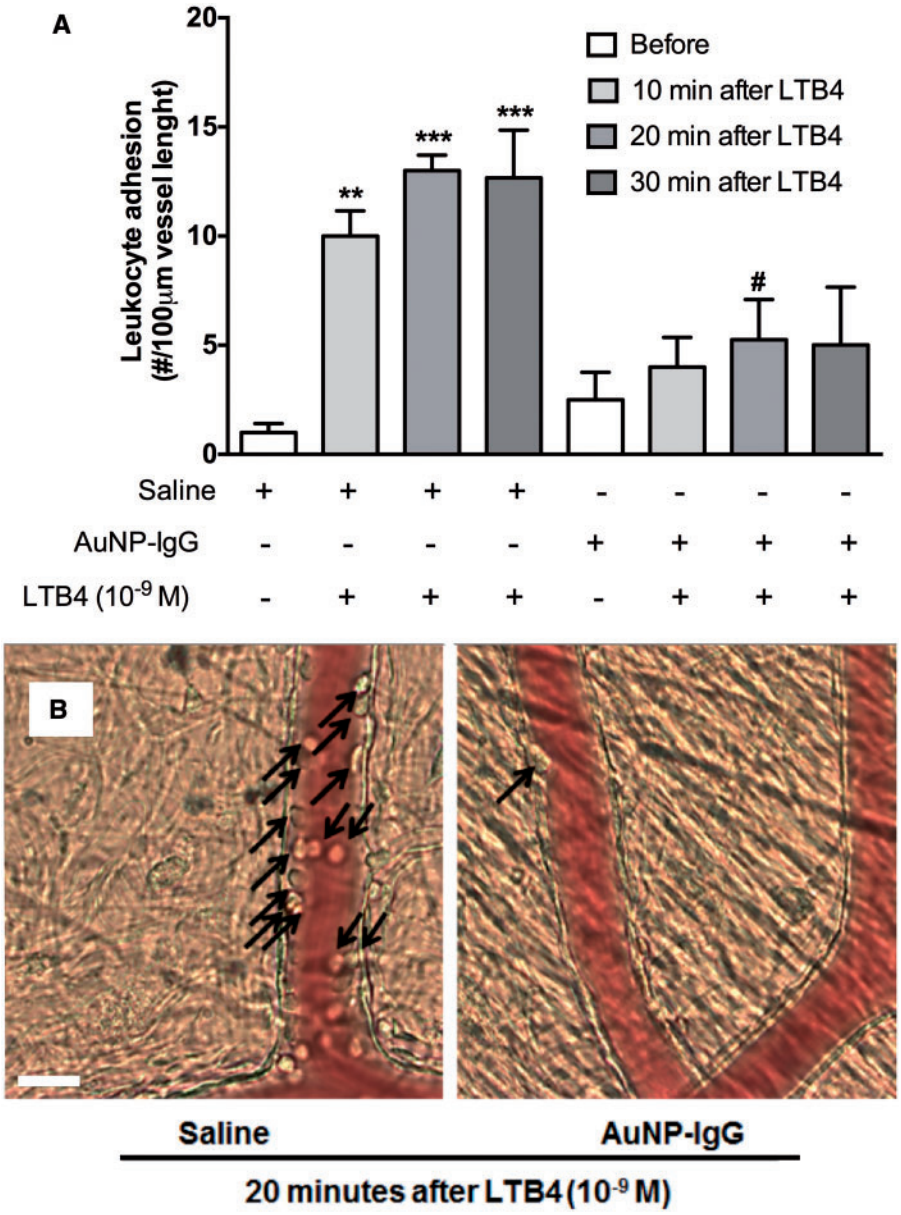

FIG. 4. Effects of gold nanoparticle-immunoglobulin G (AuNP-IgG) on leukocyte-endothelial interactions evoked by leukotriene B4 (LTB4) *in vivo*. Number of adhered leukocytes along the mesentery vessel walls of male Wistar rats previously treated IV with saline or AuNP-IgG and subsequently (30 min) stimulated with LTB4 (10^{-8} M; topically applied in the mesentery) (A). Representative images of the mesenteric vascular beds (B). Black arrows indicated adhered leukocytes 20 min after LTB4 application. White bar = 20 μm. Values express the average data obtained from 4 to 6 animals in each group. $^{**}P < .01$ and $^{***}P < .001$ versus saline basal; $^{\#}P < .05$ versus saline in the respective periods of time.

toxicity, because *cit*-AuNP and AuNP-IgG did not cause hemolysis, microhemorrhage or thrombus formation *in vivo*. Nevertheless, *cit*-AuNP and AuNP-IgG injection reduced significantly the leukocyte-endothelial interactions, as quantified by the reduced number of adhered leukocytes in the post-capillary venules, and the number of leukocytes migrated into adjacent tissues. As leukocyte-endothelial interactions are the initial and pivotal phenomena for the development of inflammatory processes (Kolaczkowska and Kubes, 2013), we inferred that AuNP bioconjugates could affect the leukocyte binding to the vessel walls during the early phases of inflammation. Therefore, the pro-inflammatory mediator LTB4, a product of the 5-lipoxygenase pathway of arachidonic acid metabolism, was the inflammatory tool employed to cause a time-dependent enhancement on leukocyte adhesion to the vessel walls and migration into adjacent tissues. Interestingly, pre-treatment with AuNP-IgG abrogated leukocyte adhesion to the vessel, confirming the anti-inflammatory effects in our *in vivo* model.

The interaction of circulating leukocytes with vessel walls is mediated by binding of membrane receptors expressed on both endothelium and leukocytes, named adhesion molecules (Kolaczkowska and Kubes, 2013). Therefore, AuNPs must be changing the membrane binding affinity or inhibiting intracellular mechanisms responsible for the cell adhesion and locomotion. Our results have indicated that the last hypothesis may be more plausible, because AuNP-IgG were found in the cytoplasm of rat neutrophils 1 h after incubation. In addition, previous incubation of neutrophils with AuNP-IgG inhibited the

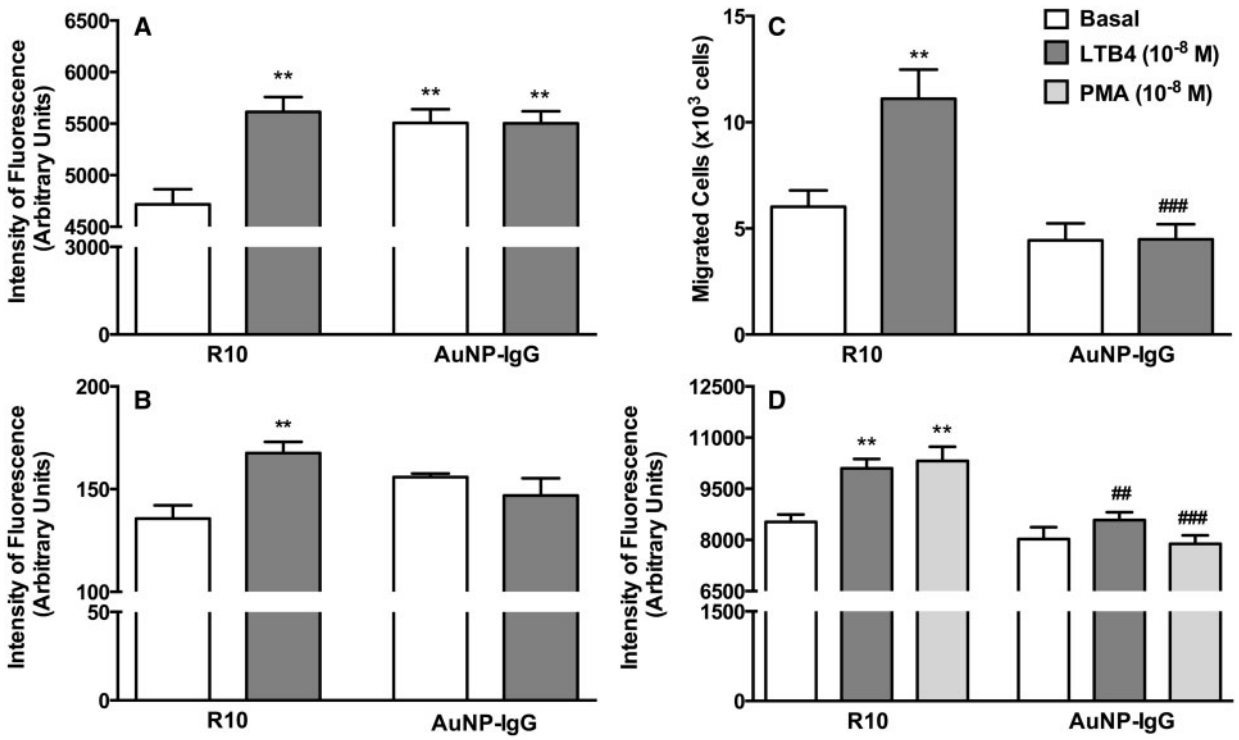

FIG. 5. Effects of gold nanoparticle-immunoglobulin G (AuNP-IgG) on neutrophils inflammatory functions. Rat neutrophils were incubated with R10 or AuNP-IgG for 2 h: A, β_2-integrin, B, PECAM expression, C, chemotactic activity and D, ROS generation. Data express mean ± s.e.m. of cells collected from four animals. $^{**}P < .01$ versus R10-Basal. $^{\#\#}P < .01$ and $^{\#\#\#}P < .001$ versus respective R10 + PMA or R10 + LTB4.

LTB4-induced oriented neutrophil locomotion. LTB4 binds to membrane G-protein-coupled receptors BLT1 and BLT2 and induces a complex intracellular cascade, resulting in neutrophil inflammatory activities (Cho *et al.*, 2011). Our hypothesis was further corroborated by the marked reduction of oxidative burst activation after treatment with AuNP-IgG in cells stimulated by LTB4 or PMA. Activation of oxidative burst is a mechanism displayed by phagocytes, such as neutrophils and macrophages, to kill engulfed microorganisms at the inflammation sites. In contrast with LTB4, PMA penetrates into cells and activates isoforms of kinases involved in the oxidative burst activation (Cho *et al.*, 2011). In conclusion, our data showed that acute exposure to AuNP-IgG did not induce toxic effects to the vascular system and cause anti-inflammatory effects in circulating neutrophils. Thus, the mechanism of action may include effects on intracellular pathways of the inflammatory process. However, the long-term effects of chronic exposure remain to be studied.

The role of AuNPs on inflammation is controversial and it may be dependent on particle size and the administration route. Whereas local anti-inflammatory effects have been reported in several experimental disease models such as arthritis and uveitis (Leonaviciene *et al.*, 2012; Pereira *et al.*, 2012), systemic administration of AuNPs was shown to cause both pro- and anti-inflammatory effects (Chen *et al.*, 2013; Khan *et al.*, 2013). Here, we showed for the first time that IV injection of AuNP bioconjugates causes anti-inflammatory effects by modifying the profile of circulating leukocytes.

The anti-inflammatory properties of gold salts have been proposed long time ago, especially for the treatment of diseases such as rheumatoid arthritis, psoriasis and gout. Although effective, they were no longer fully continued because of several adverse effects (Pedersen *et al.*, 2014). In this context, new formulations of gold salts and ions have been proposed (Larsen *et al.*, 2008) and our data may address novel possibilities to treat inflammatory diseases, especially by conjugating AuNPs with other drugs and specific membrane molecules.

In summary, the low or non-significant toxicity of AuNP bioconjugates found *in vitro* (no immune response and no cytotoxicity in human PBMC, PMN, erythrocytes and HUVEC), was confirmed in our *in vivo* model, in the microcirculation of male Wistar rats, where no change was observed in blood flow velocity, coagulation, micro-hemorrhage or thrombus. Interestingly enough anti-inflammatory properties were observed *in vivo* for the first time, as indicated by the reduced leukocyte-endothelium interaction and leukocyte influx to adjacent tissues after LTB4 stimulation. This hypothesis was further corroborated *in vitro* by the marked reduction of chemotaxis and oxidative burst activation of rat neutrophils after treatment of cells stimulated by LTB4 or PMA with AuNP-IgG. These results bring new insights and expectations on the potential application of nanobiomaterials based on AuNPs conjugated with biomolecules aiming disease treatment, diagnosis, and targeted delivery of drugs.

SUPPLEMENTARY DATA

Supplementary data are available online at http://toxsci.oxfordjournals.org/.

FUNDING

Fundação de Amparo a Pesquisa do Estado de São Paulo (FAPESP 2009/08584-6 and 2011/19595-9).

ACKNOWLEDGMENTS

The authors would like to acknowledge all the volunteers that kindly donated blood samples for the experiments. MKU and CCD are PhD fellows and SFR is a postdoctoral fellow of FAPESP [projects 2010/50072-0, 2010/19802-1, and 2011/02438-8, respectively].

REFERENCES

Araki, K., Mizuguchi, E., Tanaka, H., and Ogawa, T. (2006). Preparation of very reactive thiol-protected gold nanoparticles: revisiting the Brust-Schiffrin method. *J. Nanosci. Nanotechnol.* **6**, 708–712.

Berger, M. (2013). Adverse effects of IgG therapy. *J. Allergy Clin. immunol. Pract.* **1**, 558–566.

Bkaily, G., Al-Khoury, J., and Jacques, D. (2014). Nuclear membranes Gpcrs: implication in cardiovascular health and diseases. *Curr. Vasc. Pharmacol.* **12**, 215–222.

Bleher, R., Kandela, I., Meyer, D. A., and Albrecht, R. M. (2008). Immuno-EM using colloidal metal nanoparticles and electron spectroscopic imaging for co-localization at high spatial resolution. *J. Microsc.* **230**, 388–395.

Boyum, A. (1968). Isolation of mononuclear cells and granulocytes from human blood. Isolation of monuclear cells by one centrifugation, and of granulocytes by combining centrifugation and sedimentation at 1 g. *Scand. J. Clin. Lab. Invest.* **97**, 77–89.

Chen, H., Dorrigan, A., Saad, S., Hare, D. J., Cortie, M. B., and Valenzuela, S. M. (2013). In vivo study of spherical gold nanoparticles: inflammatory effects and distribution in mice. *PloS One* **8**, e58208.

Chithrani, B. D., Ghazani, A. A., and Chan, W. C. W. (2006). Determining the size and shape dependence of gold nanoparticle uptake into mammalian cells. *Nano Lett.* **6**, 662–668.

Cho, K. J., Seo, J. M., and Kim, J. H. (2011). Bioactive lipoxygenase metabolites stimulation of NADPH oxidases and reactive oxygen species. *Mol. Cells* **32**, 1–5.

Choi, J.-W., Kang, D.-Y., Jang, Y.-H., Kim, H.-H., Min, J., and Oh, B.-K. (2008). Ultra-sensitive surface plasmon resonance based immunosensor for prostate-specific antigen using gold nanoparticle-antibody complex. *Coll. Surf. Physicochem. Eng. Aspects* **313–314**, 655–659.

Connor, E. E., Mwamuka, J., Gole, A., Murphy, C. J., and Wyatt, M. D. (2005). Gold nanoparticles are taken up by human cells but do not cause acute cytotoxicity. *Small* **1**, 325–327.

Daniel, M. C. and Astruc, D. (2004). Gold nanoparticles: assembly, supramolecular chemistry, quantum-size-related properties, and applications toward biology, catalysis, and nanotechnology. *Chem. Rev.* **104**, 293–346.

de Assis, D. N., Mosqueira, V. C., Vilela, J. M., Andrade, M. S., and Cardoso, V. N. (2008). Release profiles and morphological characterization by atomic force microscopy and photon correlation spectroscopy of 99mTechnetium-fluconazole nanocapsules. *Int. J. Pharm.* **349**, 152–160.

de Lima, C. B., Tamura, E. K., Montero-Melendez, T., Palermo-Neto, J., Perretti, M., Markus, R. P., and Farsky, S. H. (2012). Actions of translocator protein ligands on neutrophil adhesion and motility induced by G-protein coupled receptor signaling. *Biochem. Biophys. Res. Commun.* **417**, 918–923.

Dragoni, S., Franco, G., Regoli, M., Bracciali, M., Morandi, V., Sgaragli, G., Bertelli, E., and Valoti, M. (2012). Gold nanoparticles uptake and cytotoxicity assessed on rat liver precision-cut slices. *Toxicol. Sci.* **128**, 186–197.

Faulk, W. P. and Taylor, G. M. (1971). An immunocolloid method for the electron microscope. *Immunochemistry* **8**, 1081–1083.

Forsgren, A. and Sjoquist, J. (1966). "Protein A" from S. aureus. I. Pseudo-immune reaction with human gamma-globulin. *J. Immunol.* **97**, 822–827.

Giordano, R., Fouts, D. L., Tewari, D., Colli, W., Manning, J. E., and Alves, M. J. (1999). Cloning of a surface membrane glycoprotein specific for the infective form of Trypanosoma cruzi having adhesive properties to laminin. *J. Biol. Chem.* **274**, 3461–3468.

Goodman, C. M., McCusker, C. D., Yilmaz, T., and Rotello, V. M. (2004). Toxicity of gold nanoparticles functionalized with cationic and anionic side chains. *Bioconjugate Chem.* **15**, 897–900.

Grasseschi, D., Zamarion, V. M., Araki, K. and Toma, H. E. (2010). Surface enhanced Raman scattering spot tests: a new insight on Feigl's analysis using gold nanoparticles. *Anal. Chem.* **82**, 9146–9149.

He, Z., Liu, J., and Du, L. (2014). The unexpected effect of PEGylated gold nanoparticles on the primary function of erythrocytes. *Nanoscale* **6**, 9017–9024.

Khan, H. A., Abdelhalim, M. A., Alhomida, A. S. and Al Ayed, M. S. (2013). Transient increase in IL-1beta, IL-6 and TNF-alpha gene expression in rat liver exposed to gold nanoparticles. *Genet. Mol. Res.* **12**, 5851–5857.

Kolaczkowska, E. and Kubes, P. (2013). Neutrophil recruitment and function in health and inflammation. *Nat. Rev. Immunol.* **13**, 159–175.

Kong, B., Seog, J. H., Graham, L. M. and Lee, S. B. (2011). Experimental considerations on the cytotoxicity of nanoparticles. *Nanomedicine (Lond)* **6**, 929–941.

Larsen, A., Kolind, K., Pedersen, D. S., Doering, P., Pedersen, M. O., Danscher, G., Penkowa, M. and Stoltenberg, M. (2008). Gold ions bio-released from metallic gold particles reduce inflammation and apoptosis and increase the regenerative responses in focal brain injury. *Histochem. Cell Biol.* **130**, 681–692.

Lauterwasser, C. (2005). Opportunities and risks of nanotechnologies: small sizes that matter. *Organisation for Economic Co-operation and Development (OECD)*. Avaliable at: www.oecd.org/science/nanosafety/37770473.pdf. Accessed October 8, 2014.

Leonaviciene, L., Kirdaite, G., Bradunaite, R., Vaitkiene, D., Vasiliauskas, A., Zabulyte, D., Ramanaviciene, A., Ramanavicius, A., Asmenavicius, T. and Mackiewicz, Z. (2012). Effect of gold nanoparticles in the treatment of established collagen arthritis in rats. *Medicina* **48**, 91–101.

Liz-Marzan, L. M. (2004). Nanometals: formation and color. *Mater. Today* **7**, 26–31.

Macedo, S. M., Lourenco, E. L., Borelli, P., Fock, R. A., Ferreira, J. M., Jr. and Farsky, S. H. (2006). Effect of in vivo phenol or hydroquinone exposure on events related to neutrophil delivery during an inflammatory response. *Toxicology* **220**, 126–135.

Paino, I. M., Marangoni, V. S., de Oliveira, R. C. S., Antunes, L. M. and Zucolotto, V. (2012). Cyto and genotoxicity of gold nanoparticles in human hepatocellular carcinoma and peripheral blood mononuclear cells. *Toxicol. Lett.* **215**, 119–125.

Park, K., Lee, S., Kang, E., Kim, K., Choi, K. and Kwon, I. C. (2009). New generation of multifunctional nanoparticles for cancer imaging and therapy. *Adv. Funct. Mater.* **19**, 1553–1566.

Pattan, G. and Kaul, G. (2012). Health hazards associated with nanomaterials. *Toxicol. Ind. Health* **30**, 499–519.

Pedersen, D. S., Locht, L. J., Trana, T. P., Markholt, S., Rungby, J. and Larsen, A. (2014). Toxicological aspects of injectable gold-hyaluronan combination as a treatment for neuroinflammation. *Histol. Histopathol.* **4**, 447–456.

Pereira, D. V., Petronilho, F., Pereira, H. R., Vuolo, F., Mina, F., Possato, J. C., Vitto, M. F., de Souza, D. R., da Silva, L., da Silva Paula, *et al.* (2012). Effects of gold nanoparticles on endotoxin-induced uveitis in rats. *Invest. Ophthalmol. Vis. Sci.* **53**, 8036–8041.

Sharma, P. and Sharma, J. D. (2001). In vitro hemolysis of human erythrocytes by plant extracts with antiplasmodial activity. *J. Ethnopharmacol.* **74**, 239–243.

Siddiqi, N. J., Abdelhalim, M. A., El-Ansary, A. K., Alhomida, A. S. and Ong, W. Y. (2012). Identification of potential biomarkers of gold nanoparticle toxicity in rat brains. *J. Neuroinflamm.* **9**, 123.

Sonavane, G., Tomoda, K. and Makino, K. (2008). Biodistribution of colloidal gold nanoparticles after intravenous administration: effect of particle size. *Coll. Surf. B. Biointerfaces* **66**, 274–280.

Stefan, M., Melnig, V., Pricop, D., Neagu, A., Mihasan, M., Tartau, L. and Hritcu, L. (2013). Attenuated effects of chitosan-capped gold nanoparticles on LPS-induced toxicity in laboratory rats. *Mater. Sci. Eng. C* **33**, 550–556.

Tarantola, M., Schneider, D., Sunnick, E., Adam, H., Pierrat, S., Rosman, C., Breus, V., Soennichsen, C., Basche, T., Wegener, J., *et al.* (2009). Cytotoxicity of metal and semiconductor nanoparticles indicated by cellular micromotility. *ACS Nano* **3**, 213–222.

Turkevich, J., Stevenson, P. C. and Hillier, J. (1951). A study of the nucleation and growth processes in the synthesis of colloidal gold. *Discuss. Faraday Soc.* **11**, 55–75.